Liquid Crystals
Publication details, including instructions for authors and subscription information:
http://www.informaworld.com/smpp/title~content=t713926090

A new image processing method for enhancing the detection sensitivity of smooth transitions in liquid crystals

B. Montrucchio; A. Sparavigna; A. Strigazzi

Online publication date: 06 August 2010

To cite this Article Montrucchio, B. , Sparavigna, A. and Strigazzi, A.(1998) 'A new image processing method for enhancing the detection sensitivity of smooth transitions in liquid crystals', Liquid Crystals, 24: 6, 841 — 852
To link to this Article: DOI: 10.1080/026782998206669
URL: http://dx.doi.org/10.1080/026782998206669

LIQUID CRYSTALS, 1998, VOL. 24, NO. 6, 841–852

A new image processing method for enhancing the detection sensitivity of smooth transitions in liquid crystals

by B. MONTRUCCHIO, A. SPARAVIGNA†* and A. STRIGAZZI†

Centro Servizi Informatici e Telematici, Politecnico di Torino,
C.so Duca degli Abruzzi 24, 10129 Torino, Italy
†Dipartimento di Fisica and Istituto Nazionale di Fisica della Materia (INFM),
Politecnico di Torino, C.so Duca degli Abruzzi 24, 10129 Torino, Italy

(*Received 5 January 1998; accepted 23 January 1998*)

A study of textural changes is presented concerning the nematic phase of 4-*n*-alkyloxybenzoic acids (in particular, 4-*n*-heptyl- and 4-*n*-octyl-oxybenzoic acids), by means of a statistical approach to the image data observed by polarized light microscopy (orthoscopic mode). A new image processing method is developed in order to detect with high sensitivity any structural change in the image frame. To do this, a set of parameters is introduced, charaterizing the observed textures. Such a set is a vector, working like a pathfinder strongly increasing the human eye—or in general the sensor—skilfulness to appreciate any change of the optical texture, both in space and in time. This is suitable for revealing smooth transitions, such as phase transitions between smectic and nematic phases (or between different smectic phases), or order transitions, like alignment transitions in poorly oriented nematic layers. In fact, by using this method for detecting the order transition between two nematic 'subphases' of 4-*n*-alkyloxybenzoic acids, the sensitivity turns out to be enhanced by a factor higher than 10 with respect to that for standard techniques. The new method allows us to define a characteristic size of the image texture: this concept is applied to analyse several image data for estimating the mean size of the domains appearing in the smectic and in the nematic phase of the compounds under study.

1. Introduction

The image is an essential carrier of information in many technological applications and in scientific research as well. Digital image processing is a multidisciplinary field in the course of rapid development due to the improvement rate in computer hardware and in CCD devices for image acquisition. The goals are enhancement in the speed, storage capability, resolution, accuracy and reliability of the image encoding, restoration and analysis [1].

Experimental research in the field of liquid crystals by means of polarized light microscopy in the orthoscopic mode mainly needs to describe and analyse both pattern (textures and defects) and areal uniformity (in brightness and in colour). As a consequence, digital image processing can be regarded as a fundamental tool for the recognition of the typical patterns which characterize samples of mesogens when, for instance, the mesophase undergoes some periodic features [2] or for establishing the degree of areal uniformity when the anisotropic samples under study exhibit a well defined alignment whose accuracy has to be checked [3].

*Author for correspondence.

In image processing science, several methods have been developed for classifying images and for defining the statistical distances between them, with the aim of deciding whether, in a set of many images, there exist some which are close, within a prefixed accuracy, to one arbitrary image previously given. Texture discrimination, for instance, can be done by choosing a family of attributes which account for the main spatial organization of the image. In general, the model underlying the attributes can be either structural or statistical. In the first case, a texture is characterized by a family of primitives and by their spatial organization [4]. In the second case, the use of statistical tools is involved and the textural features can be derived from the Fourier power spectrum of the image [4, 5]. After that, the texture discrimination requires a suitable definition of distance, a concept which is introduced to describe the difference between texture attributes as a whole [6, 7].

Many sophisticated procedures for reconstruction of a 3-dimensional scene from a 2-dimensional projection have also been developed [8]: one application is, for instance, the reconstruction of a depth map from a focus series relevant to polarizing microscopy [9].

0267–8292/98 $12·00

Our point of view is that all these techniques can be very useful in the field of liquid crystal investigations using polarized light microscopy, where it is well known that the analysis of slides using only human abilities, or even detectors, but giving simply a picture-like representation (locally sensitive to brightness, colour and contrast), is time consuming and involves severe limitations concerning the type and the quality of the detectable information.

Standard polarized light microscopy of liquid crystals is devoted either to texture description (investigating transition points or characterizing phase structures) or to light intensity or optical path difference measurements in well aligned samples. According to our knowledge, image statistical treatments have never been used to fulfil such requirements.

We will show in this paper that the application of image statistical treatments to optical investigations of liquid crystal textures is essential for enhancing detection sensitivity and structure recognition. Taking as a starting point the use of statistical concepts used in the object recognition process—that is, the detection of an image embedded in a background or the recognition of some object differing from a background consisting of many other objects [10, 11]—we have developed an image processing technique that provides a set of statistical parameters characterizing not only the intensity of the image as a whole, but also the possible anisotropy and coarseness of the image texture.

Let us stress that the image can consist of several objects (in the case where either defects or relatively small domains are present) or of one object (in the case when uniformity prevails). In both situations, we consider the position and dispersion indices, i.e. the mean intensity of the transmitted light (averaged over the whole window, which can be the entire beam cross section, or a certain part of it) and the kth order moments of the light intensity distribution (with $k = 1, n$ with n defined *a priori*) [10]. These parameters are extremely sensitive to changes in the textures of liquid crystals and thus can be very useful for the investigation of structural changes due to both order and phase transitions in the materials.

In fact, the application of the moments method to the optical investigations of (i) phase transitions (in the case of similar textures in both phases) and (ii) order transitions (within the same phase) represents a significant improvement in the detection sensitivity.

The major limitation of any moments description is that is cannot follow the local spatial character of the image frame, since this particular information is drowned in the average sea. Some of the standard techniques for texture description [10] are, for instance, based on the analysis of light intensity difference [5, 12] reported as a function of the distance from an arbitrary point of the image frame. Other methods are based on so-called 'run-length statistics' [12, 13], characterized by moving in a chosen direction from an image arbitrary point, looking for the number of pixels with the same intensity as the starting point. Instead, in the frame of the moments calculation, we propose a new approach, with the aim of defining a size characterizing the different textures observed under various conditions, and estimating this size. By means of our statistics, a characterization can easily be obtained of the anisotropy and coarseness to be attributed to the smectic and the nematic phases of mesogenic compounds, even in cases where standard techniques were not able to give significant results.

To check the reliability of the method, we have applied it to the optical investigation of the phase and order changes in homologous 4-*n*-alkyloxybenzoic acids: specifically 4-*n*-heptyl- and 4-*n*-octyl-oxybenzoic acids, commonly denoted in the literature as 7OBAC and 8OBAC, respectively, or sometimes as HOBA and OOBA, respectively.

These materials exhibit both smectic C and nematic phases [14, 15]. The nematic phases are affected by two different orderings, at low and high temperatures revealing themselves as two 'subphases' N_1 and N_2, respectively, characterized by different textures. Hence, any optical microscopy is affected by images having different features. In fact, the low temperature 'subphase' N_1 occurs on heating from a smectic C phase and has a well defined molecular ordering, which is higher with respect to the N_2 phase. This was interpreted as due to the presence of cybotactic clusters having short range smectic C ordering [16].

In effect, in the alkyloxybenzoic acids the mesomorphic behaviour depends upon the presence of closed dimers, provided by intermolecular hydrogen bonds [17], at a concentration high enough to ensure long range nematic ordering (at high temperature), and a mean range smectic ordering (at a lower temperature) [14]. Of course, at high temperatures in the nematic phase, the dimer concentration is lower than that necessary for obtaining the smectic ordering. At lower temperatures in the nematic phase, the dimers aggregate in clusters having a mean range smectic C ordering (a pre-transitional effect) [16]. This smectic-like ordering has been found to influence the dielectric and thermal properties of the nematic phase [18], as well as the optical properties.

Recently, the order transition between the N_1 and N_2 'subphases' in 4-*n*-heptyloxybenzoic acid has been studied by optical microscopy and X-ray investigation [19] and the influence of a twist distortion on the transition temperature has been determined [20]. For this purpose, a special surface treatment of the glass

plates of the liquid crystal cell was used, ensuring a pretilt at both cell substrates in order to make the transition more easily observable.

However, in the optical measurements here presented, no particular treatment of the glass plates was used. In this situation, polarized light microscopy observations by visual inspection, relevant to the critical temperature T_c between the two nematic 'subphases', proved to be more easily identifiable on cooling from the isotropic phase than on heating from the smectic phase. Instead, we will show here that using the present statistical approach to the data, the critical temperature is equally readily detected, and with higher sensitivity, in both cases. This demonstrates the power of the proposed method for assisted measurement of transition temperatures by means of a simple statistical analysis of the image.

2. Experimental set-up

The experiment involved polarized light microscopy in the orthoscopic mode. The cells used were of the common sandwich type, with a gap of 23 μm, ensured by mylar spacers. The liquid crystal material was introduced into the cells in the isotropic phase by capillarity. The inner surfaces of the cell substrates (glass plates) were simply rubbed in order to favour a unidirectional planar alignment in one privileged direction. The sample was mounted in a Linkam hot stage and the temperature was controlled within an accuracy of 0·1°C.

The optical investigation was carried out using a Leitz polarizing microscope. A JVC colour CCD camera with fixed shutter was used for recording the observations: the digital image acquisition from the camera was made by a colour video digitizer (Play Incorporated) driven by a computer. The JVC camera was simultaneously connected to a Grundig SVHS video recorder.

The observed transition temperatures for 7OBAC and 8OBAC are shown in the table. They are in agreement with those reported in the literature by several authors [18, 19, 21–25]. On cooling, the previously observed hysteresis of the critical temperatures for 7OBAC [20] and for 8OBAC [19] are confirmed here.

Table. Transition temperatures in °C for 7OBAC and 8OBAC on heating and on cooling: note the hysteresis on cooling.

Compound	Phase transition			
Heating	Cr–SmC	SmC–N_1	N_1–N_2	N_2–I
7OBAC	90	96	116	142
8OBAC	98	105	122	140
Cooling	I–N_2	N_2–N_1	N_1–SmC	SmC–Cr
7OBAC	139	113	93	87
8OBAC	137	116	102	93

In figure 1, typical textures of the smectic phase and of the nematic N_1 and N_2 'subphases' are shown for 7OBAC. The smectic phase exhibits a sand-like, domain structure: nematic N_1 looks like a sandy beach after passage of a gentle wave, and, finally, nematic N_2 has a uniform well aligned orientation. In both nematic 'subphases', areas with different birefringence can be observed: in N_1, the single domains appear as small spots, whereas in N_2 there are large zones with small differences in transmitted light [26].

Sometimes, on cooling from the isotropic phase, a much less pronounced marbled texture persisted in the smectic phase, if such a texture is present for the precursor nematic phases. In figure 2 the evolution of the defects on cooling from the high temperature 'subphase' N_1 (*a*) to the 'subphase' N_2 (*b*) and from N_2 to the smectic phase (*c*) is shown.

At the critical temperature T_c between the two nematic 'subphases', spots start to disappear on heating or to appear on cooling: this effect is more pronounced on cooling, and is easier to observe in this case by simple visual inspection.

For 8OBAC the transition between the N_1 and N_2 'subphases' is more evident. The texture in the smectic phase and in the nematic N_1 'subphase' is again sand-like as observed for 7OBAC.

3. Image analysis and discussion

Through the signal coming from the video digitizer, the true colour image detected by the CCD camera is stored in a file with a resolution of 640×480 pixels. The file is elaborated on a Digital Alpha Workstation DEC255 by an original C-program made in the frame of this work, that reads and analyses the image, choosing one of the three fundamental colours (red, green and blue). In our case we chose the most sensitive colour, which is green, even although quite similar results would be obtained simply by translating the whole RGB image into a unique integrated image exhibiting a grey-scale.

To each pixel at the arbitrary point $P(x, y)$ in the image frame our C-program associates a green tone b ranging from 0 to 255: $b(x, y)$ is then a 2-dimensional function representative of the image intensity (brightness) distribution. The number of pixels N of colour tone b can be represented in histogram, transforming in this way the 2-dimensional information into a 1-dimensional description: in figure 3, the histograms of the three images already reported in figure 1 are shown, with the maximum number of pixels on the y-axis normalized to 255.

Starting from the function $b(x, y)$, which gives the pixel colour tone, the following calculations can be performed. First of all, the mean intensity of the colour

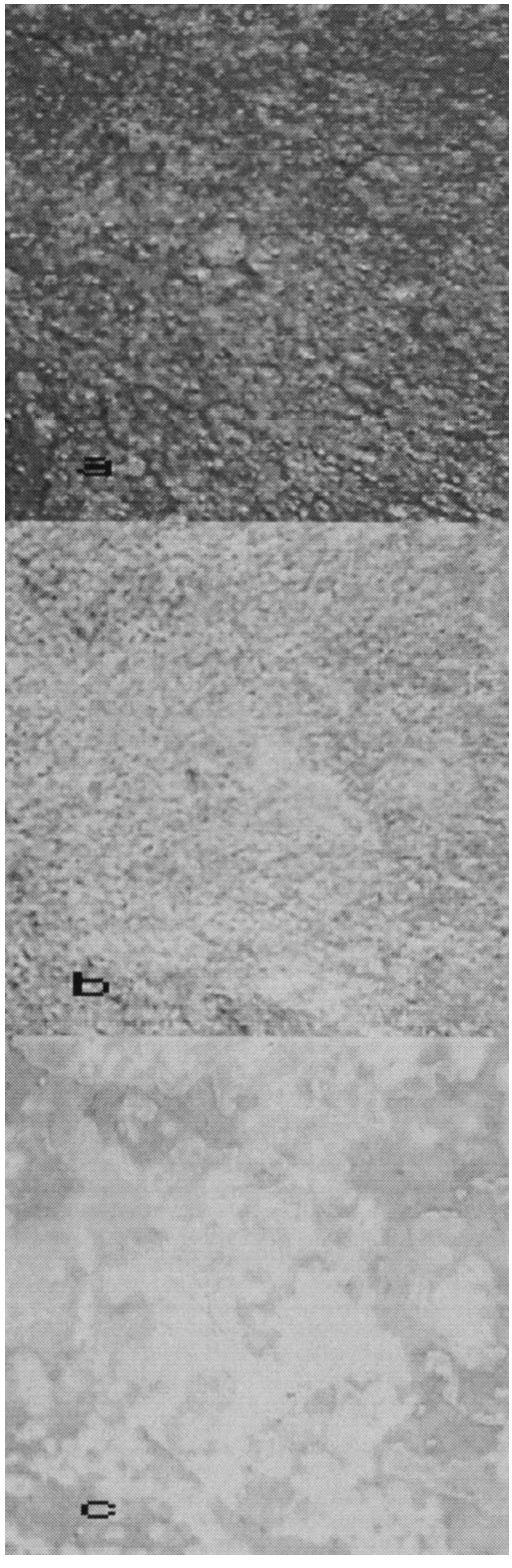

Figure 1. Textures of 7OBAC in the smectic C phase at 92°C (*a*) and in the two nematic 'subphases' at low (*b*) and high (*c*) temperatures, 110°C and 130°C, respectively: the sand-like texture is easily recognizable in the smectic (*a*) and in the N_1 'subphase' (*b*). The high temperature nematic phase (*c*) is composed of almost uniform areas. The size of each figure is $500 \times 500\,\mu m^2$.

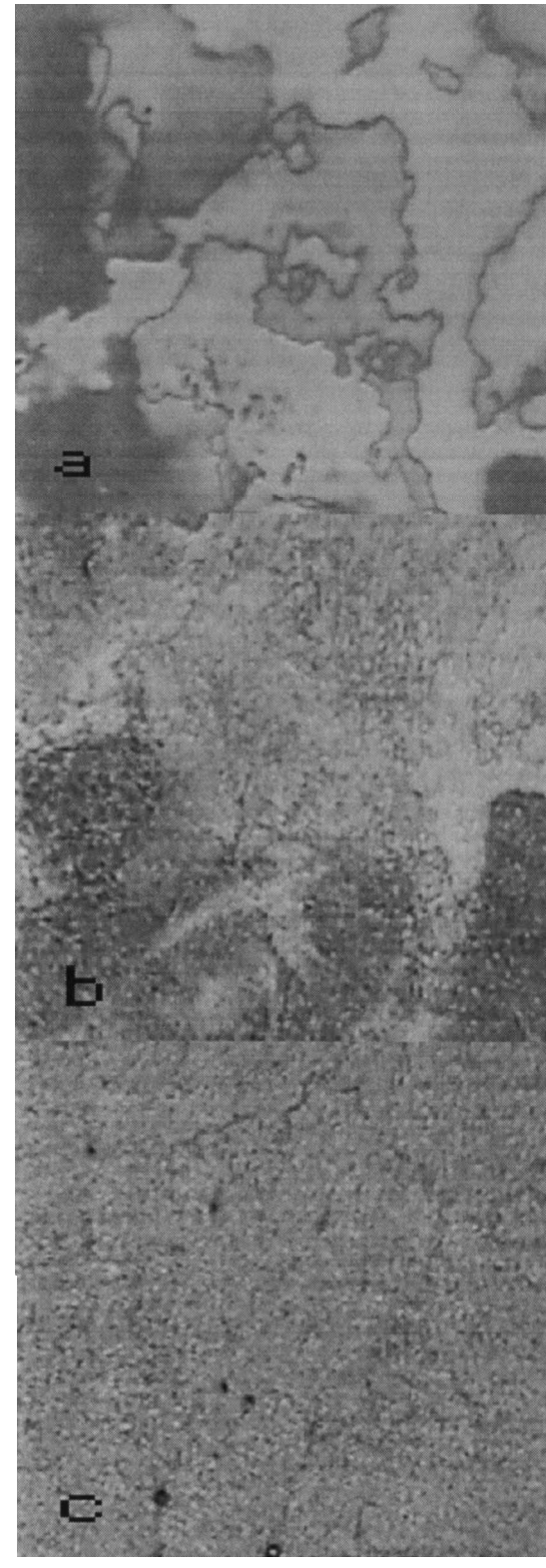

Figure 2. Defect textures in 7OBAC on cooling from the isotropic phase in the high 'subphase' N_2 (*a*), and in the low temperature nematic 'subphase' N_1 (*b*), at 130°C and 110°C, respectively. In the smectic phase (*c*) the defects are also present. The size of each figure is $500 \times 500\,\mu m^2$.

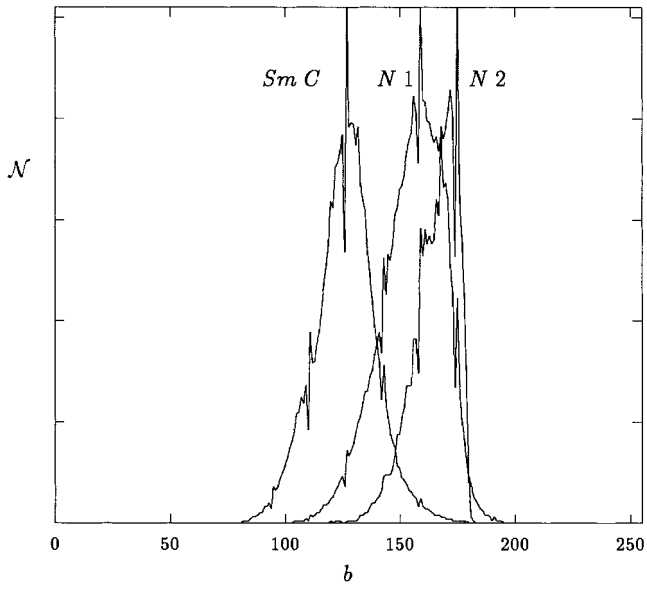

Figure 3. Number of pixels N as a function of the colour tone b for the smectic and the two nematic phases shown in figure 1: the maximum number N is normalized to 255.

tones is calculated:

$$M_0 = \frac{1}{l_x l_y} \int_0^{l_x} \int_0^{l_y} b(x, y)\, \mathrm{d}x\, \mathrm{d}y \qquad (1)$$

where l_x, l_y are the x and y rectangular range of the image frame.

The k-rank statistical moments of the image are defined in the following way:

$$M_k = \frac{1}{l_x l_y} \int_0^{l_x} \int_0^{l_y} [b(x, y) - M_0]^k\, \mathrm{d}x\, \mathrm{d}y. \qquad (2)$$

This kind of characterization has been chosen since in the majority of the observations on 7OBAC and 8OBAC the nematic and smectic phases look more or less homogeneous (in the absence of defect features): thus we are then able to define the average intensity values for the whole image frame with a physical meaning, since the dispersion turns out to be limited within $\sim 10\%$ of the average. All integrals can be calculated on the whole image or on a window. In this case, the moments M_0 and M_k allow the determination of the position and of the mean shape of the object. These concepts are very useful in microscopy investigations for the detection of defects and for the recognition of non-homogeneous structures.

Since at a first glance no particular inhomogeneities are present (figure 1), we can use the same values of the moments M_0 and M_k defined by equations (1) and (2) for the whole image, supposing the image to be characterized by only one intensity distribution.

However, if the image exhibits irregular domains, either localized (defects) or not, the quality ratio between the intensity standard deviation and the mean, taken over the entire image frame, is higher than an acceptance limit, say 50%. On the other hand, in principle a domain is described by an intensity distribution which can differ essentially from the others or from the background distribution. In this case, it is misleading to start from the point of view that only one distribution is enough to describe the whole image frame. On the contrary, it is necessary in this case to share the image in a lattice of windows, where inside each window the quality ratio is lower than the acceptance limit. The subjectivity of the choice does not affect the sensitivity of the method, as the choice connected with subdividing a statistical variable range of classes does not also affect position and dispersion indices of the sample.

However, it is necessary to check whether the hypothesis of homogeneity is really verified and whether preferred directions are present in the image frame (hypothesis of isotropy). In this connection, it is interesting to introduce a typical length characterizing the texture size: we will find that this is very useful for both smectic and nematic phases.

Instead of measuring the homogeneity, by evaluating the histogram's entropy of intensity difference versus distance from a point of the image frame (see for instance [10]), or by calculating the spatial organization by means of 'run-length statistics' [12, 13], we have computed a set of coherence lengths defined in the following way. Starting from an arbitrary point $\mathrm{P}(x, y)$ of the figure $b(x, y)$, along the eight radial directions at 45 degrees each from the other we calculated the mean value $M_0^i(x, y)$ and the $M_k^i(x, y)$ moments:

$$M_0^i(x, y) = \frac{1}{l_{0i}} \int_0^{l_{0i}} b(x + r \sin \theta_i, y + r \cos \theta_i)\, \mathrm{d}r \qquad (3)$$

$$M_k^i(x, y) = \frac{1}{l_{ki}} \int_0^{l_{ki}} [b(x + r \sin \theta_i, y + r \cos \theta_i) - M_0^i(x, y)]^k\, \mathrm{d}r \qquad (4)$$

where the index i is ranging over all directions from 1 to 8, r is the radial distance from P, and θ_i is the angle formed by the i-direction with the y-axis (see figure 4).

The lengths l_{0i} and l_{ki} are the radial distances (from P) at which the values of the direction moments $M_0^i(x, y)$ and $M_k^i(x, y)$ saturate, within a threshold level τ, to the image mean moments M_0 and M_k, defining in this way the local coherence lengths $l_{0i}(x, y)$ and $l_{ki}(x, y)$ of the image frame.

A natural choice of the threshold τ depends on the problem under study: in the investigation of the textural

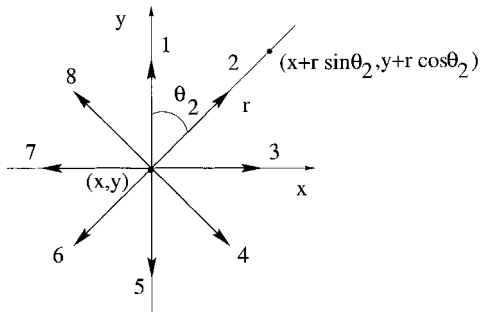

Figure 4. Reference system used in the calculation of the mean value $M_0^i(x, y)$ and the moments $M_n^i(x, y)$ along the i-direction. The index i ranges from 1 to 8.

changes corresponding to order transition, it is straightforward to assume it to be a little smaller than the percentage variation of the transmitted light intensity on moving from the N_1 to the N_2 'subphase'. For instance, for 7OBAC, it turns out to be about 5%.

In our case, the evaluation of the intensity difference as a function of the distance from an arbitrary point of the image frame, and the related distribution entropy are not able to give information on the possible anisotropy of the image in the nematic N_1 and N_2 'subphases', due to the weak intensity variation in the image frame. On the other hand, the so-called 'run-length statistics' procedure is useful only for the N_2 nematic 'subphase' with a practically uniform intensity.

In the calculation of the functions $l_{0i}(x, y)$ and $l_{ki}(x, y)$, we did not take into account the pixels near the image frame boundary, since in this case it would not be possible to estimate $l_{0i}(x, y)$, $l_{ki}(x, y)$ in all the eight directions (boundary effect).

On the contrary, in some standard image processing techniques [8], cyclicity of the image, originally present or artificially introduced by replication of the frame, is used to overcome the boundary problem; however, in our case, this procedure would be equivalent to introducing some defects into the image, since the presence of these replicas would produce as a consequence an anomalous behaviour of the coherence functions $l_{0i}(x, y)$ and $l_{ki}(x, y)$.

Moreover, in our case the moments $M_0^i(x, y)$, $M_k^i(x, y)$ were not calculated over a window as a surface, but along eight directions (if the image had mirror symmetry, we could integrate only along four directions): therefore our method is different from the standard statistical approach, allowing us to take naturally into account the anisotropy in the problem of texture recognition.

Actually, we have looked for anomalous behaviour of the vector $l_{0i}(x, y)$, $l_{ki}(x, y)$ such as a signal of a defect presence in a certain position inside the sample, corresponding to a given point $P(x, y)$ of the image frame.

To discuss what can be properly considered as an anomalous behaviour of the coherence lengths, let us introduce the following mean values of the coherence lengths along the eight directions, averaged over all the window:

$$L_{0i} = \frac{1}{l_x l_y} \int_0^{l_x} \int_0^{l_y} l_{0i}(x, y)\, \mathrm{d}x\, \mathrm{d}y \tag{5}$$

$$L_{ki} = \frac{1}{l_x l_y} \int_0^{l_x} \int_0^{l_y} l_{ki}(x, y)\, \mathrm{d}x\, \mathrm{d}y. \tag{6}$$

If the image frame were strictly homogeneous, such averaged lengths should coincide with the actual local lengths measured for all image points. On the other hand, if the image frame were completely inhomogeneous, the local lengths would be very dispersed around their averages. The same occurs when the image frame is shared in windows, each of them characterized by a different intensity distribution. It is acceptable to average the coherence length over the whole image frame if the image is characterized by one distribution only, with a reasonable dispersion. In the present case, the coherence lengths allow us to determine the averaged anisotropy of the image.

Of course, the absence of any preferred direction in the image does not mean that there are no preferred directions in the sample structure. For instance, a unidirectionally planar aligned liquid crystal cell, viewed between crossed polarizers, will produce a uniform image (with intensity dependent on the angle between the director alignment and the polarizer plane).

In figure 5 the results of the calculation of L_{0i} for the images of figure 1 are reported (the results are in microns). Note that the curve for the nematic high temperature 'subphase' N_2 shows an approximately equal coherence distance in all the eight directions, revealing no preferential directions in the image texture.

Instead, for the smectic phase and for the nematic low temperature 'subphase' N_1, an asymmetric behaviour is clearly present. For the chosen threshold τ, the curves of figure 5 give the smallest image area having the same mean intensity of the entire image frame and could be used to define the coarseness of the texture in the xy plane. In the present case, the smectic phase has a coarseness bigger than the nematic 'subphase' N_1. The small area of the curve pertaining to 'subphase' N_2 means that the image frame is composed of large, almost uniform areas. In fact, in the case of an image frame with uniform intensity distribution $b(x, y)$, the coherence lengths L_{0i} reduce to zero and the corresponding curve to a point.

Let us suppose now that the existence of a transition is *a priori* unknown. At this point, two alternative situations can be true: either the transition does exist, or it does not. In the first case, the choice of τ is

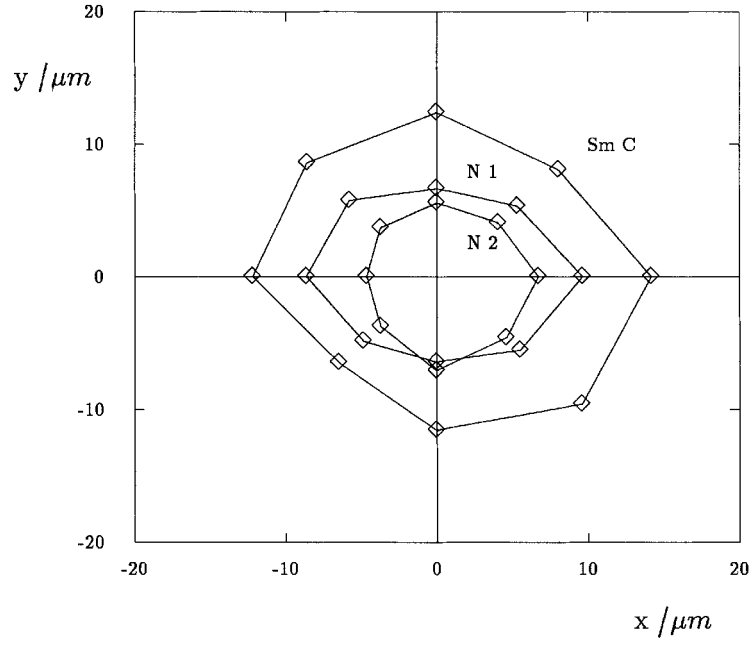

Figure 5. Values of the mean coherence lengths L_{0i} for the smectic and the two nematic 'subphases' shown in figure 1. The curves give the smallest area of the image having the same mean intensity as that of all the image frame and allow an estimation of the texture coarseness in the smectic phase and in the 'subphases' N_1 and N_2.

determining a procedure of convergence of the calculation. Instead, if the transition does not exist, there is no statistical difference between the two images, and the procedure is significantly non-convergent.

A different behaviour of the lengths L_{0i} and L_{ki} with respect to the threshold τ can be observed, in the sense that L_{0i} is greater as τ becomes smaller, until the intensity (0th moment) coherence length reaches the value of the image's greatest size, whereas the kth moment coherence lengths L_{ki} (see figure 6 for $k=2$) saturate almost at the chosen threshold level (about 5% in the case of the image in figure 1). For the sake of simplicity, we investigated this behaviour up to $n=4$. The different behaviour between L_{0i} and L_{ki} is due to the fact that the lengths L_{0i} represent the minimum distance from the generic point $\mathrm{P}(x, y)$ along the chosen direction, at which the mean value of the entire image intensity is practically reached: for this reason it is strongly dependent on the threshold level. Instead, the L_{ki} (and in particular L_{2i}) represent the minimum size of the part of the image exhibiting the same statistical dispersion (variance) as that of the whole figure.

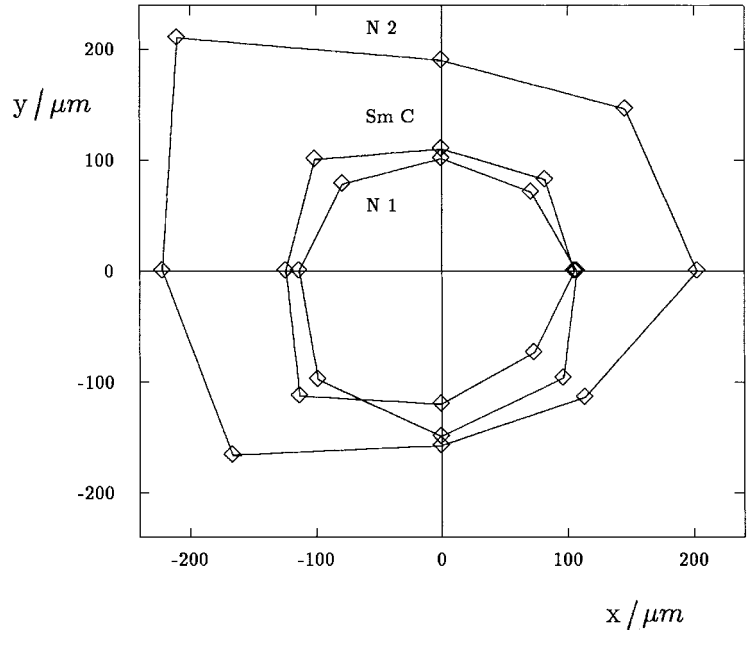

Figure 6. Values of the mean coherence lengths L_{2i} for the smectic and the two nematic 'subphases' shown in figure 1. The curves represent the smallest part of the image exhibiting the same statistical dispersion (variance) as that of the whole figure.

Let us note in figure 6 the different behaviour of the 2nd moment length in the N_2 'subphase' with respect to that in N_1 and in the smectic phase: the variance in coherence length is greater there, as compared with the values relevant to the N_1 'subphase' and to the smectic phase. This is due to the presence of several well oriented regions with different birefringent properties in 'subphase' N_2. The coherence length variance is more or less equal to the distance between the centres of the different regions. On the other hand, the existence of a large value of L_{2i} can be due to the presence of different distributions in various regions of the image frame.

As a conclusion of the discussion about coherence lengths, let us stress the fact that the mean values L_{ki} of the k-moment coherence lengths define the smallest region in the image having the same k-moment as that of the image frame as a whole.

Concerning checking the presence of defects in the image, we developed a criterion involving the local behaviour of the coherence length $l_{0i}(x, y)$. In the case of an almost homogeneous image frame, we reasonably assumed that the point $P(x, y)$ does not belong to a defect, if the mean local values $l_0(x, y) = \Sigma_i l_{0i}(x, y)/8$, for $i = 1, 8$ are included between two extremal lengths $L_0^{\min}$ and $L_0^{\max}$, where $L_0^{\min}$ is the minimum of the eight mean values of equation (5) and $L_0^{\max}$ is the maximum. Obviously, for an almost isotropic image frame, the two extremal values $L_0^{\min}$ and $L_0^{\max}$ are close together.

In figure 7 (*b*), the result of our procedure is shown, as applied to the nematic phase N_2 of figure 1 that is given here again in figure 7 (*a*) for easier comparison. In the points marked in dark grey, which are the defects, the mean local coherence lengths $l_0(x, y)$ are not comprised in the interval $[L_0^{\min}, L_0^{\max}]$. Instead, the points not belonging to defects are marked in grey, while the pale ones are points near the boundary, where it is not possible to calculate one or more of the lengths $l_{0i}(x, y)$. The dark region comprises the domains having significantly different birefringence with respect to the surrounding area. This is in agreement with the previous discussion relevant in figure 6.

With commercial software another procedure is used, consisting only in checking whether the pixel intensity is, within a fixed tolerance (for instance the standard deviation) coincident with the mean intensity of the image. This procedure is known as 'image segmentation

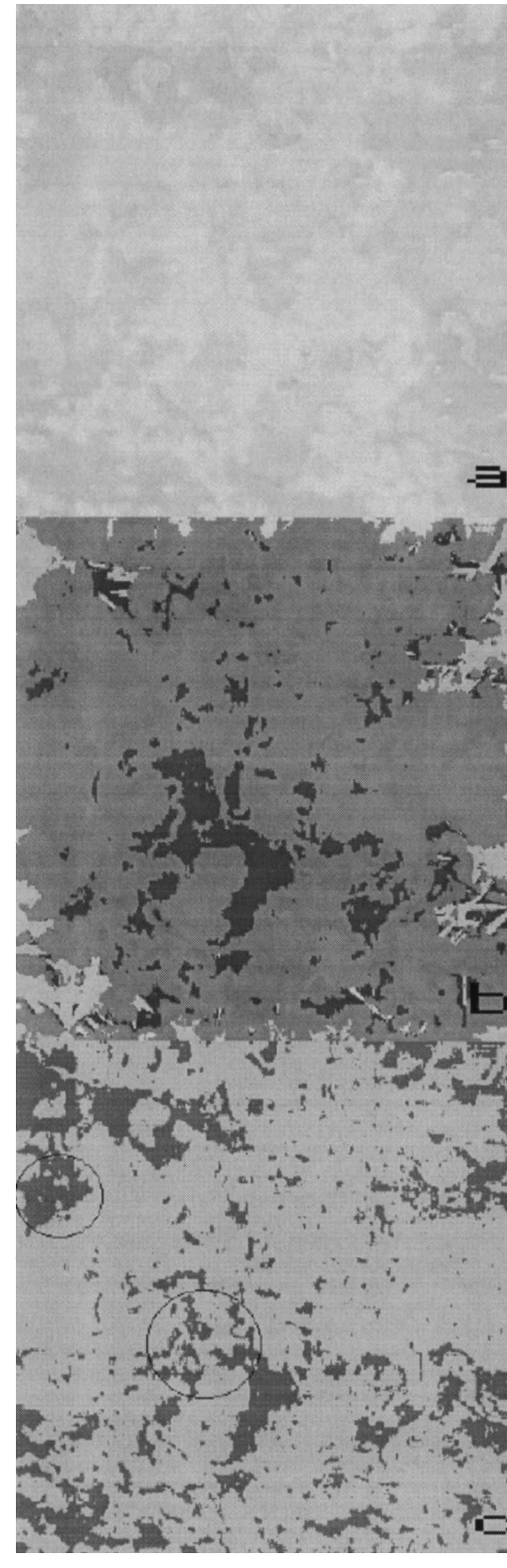

Figure 7. Result of our defect identification procedure (*b*) as applied to the nematic phase N_2 of figure 1 shown here again in (*a*) for easier comparison. The points marked in dark grey are considered 'defects' (see text for explanation). Note that the dark regions comprise domains having significantly different birefringence with respect to the surrounding area. In (*c*) comparison with the segmentation thresholding procedure is carried out with a commercial program. In the circled regions, we can see that the two procedures produce different 'defects'.

by thresholding; [10]. The image frame is segmented in two regions (light and dark) by thresholding; this consists, in the simple form we used, in constructing the following image $t(x, y)$ with

$$t(x, y) = \begin{cases} \text{light} & \text{if } b - \sigma < b(x, y) < b + \sigma \\ \text{dark} & \text{otherwise} \end{cases} \quad (7)$$

with b the mean intensity and σ the standard deviation (for the present image, the standard deviation is $\sim 5\%$). The result is shown in figure 7 (c): by comparing this image with the one in figure 7 (b), we can conclude, looking for instance at the two circled regions, that the two procedures produce different 'defects' as a consequence of the different meaning attributed to the definition of defect.

In other words the segmentation thresholding technique avoids looking for what happens around the arbitrary point, we are considering: thus, the identification of the point itself as belonging (or not) to a defect cannot be stated reliably. As an example, the nematic 'subphase' N_1, which is characterized by many small domains (spots) exhibiting relatively high intensity, would be identified by image segmentation by thresholding as a network of defects.

4. Application to the detection of transitions

We applied the proposed image technique to the high sensitivity detection of phase and order transitions in alkyloxybenzoic acids. After collecting a set of image frames of the liquid crystal cell, scanned at different temperatures, by imposing a controlled temperature rate (2 degrees per min) from room temperature till the clearing point of the material under study, for each image frame the histogram of the occurrence number N of the colour tone b is calculated.

A very useful way to present the complete set of these histograms is to map the occurrence number in grey tones g (ranging from 0 to 255 inclusive). In figure 8, the brightness occurrence during the temperature scanning of 7OBAC (on heating) is presented: it refers to the images reported in figure 1. Here the value of the colour tone b is varying along the vertical axis, and the number N is transferred into a convenient grey tone; no threshold was fixed on the vertical axis, because the image histograms fill the whole grey range, vanishing at the borders. Note that the temperature is varying along the horizontal axis and that each image map covers 4 degrees.

One can immediately recognize the transition temperatures from crystal to smectic C ($Cr \rightarrow SmC$), from smectic C to nematic ($SmC \rightarrow N_1$), the 'subphase' transition ($N_1 \rightarrow N_2$) and the clearing point ($N_2 \rightarrow I$). Let us stress that by using our analysis method all the transitions are equally detectable with high sensitivity:

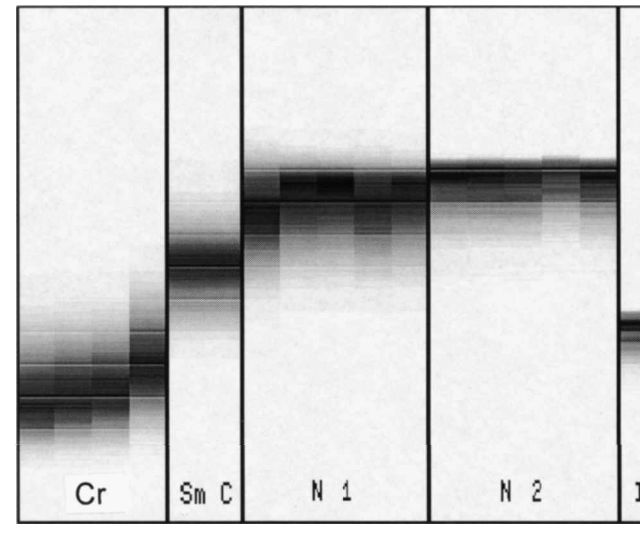

Figure 8. Brightness occurrence during temperature scanning (on heating) for 7OBAC: the transitions are at 90°C for $Cr \rightarrow SmC$, 96°C for $SmC \rightarrow N_1$, 116°C for $N_1 \rightarrow N_2$ and the clearing point is at 142°C. The value of the colour tone b varies along the vertical axis and the number N is transferred into a grey tone. The temperature varies along the horizontal axis and each image map covers 4 degrees.

in particular, the critical point $N_1 \rightarrow N_2$ (the order transition) is clearly observed.

In figure 9, the mean intensities and the variances of the histograms reported in figure 8 are denoted by the thick and thin lines, respectively: the curve representing the variances clearly shows, besides the phase transitions, the textural transition from the optically disordered

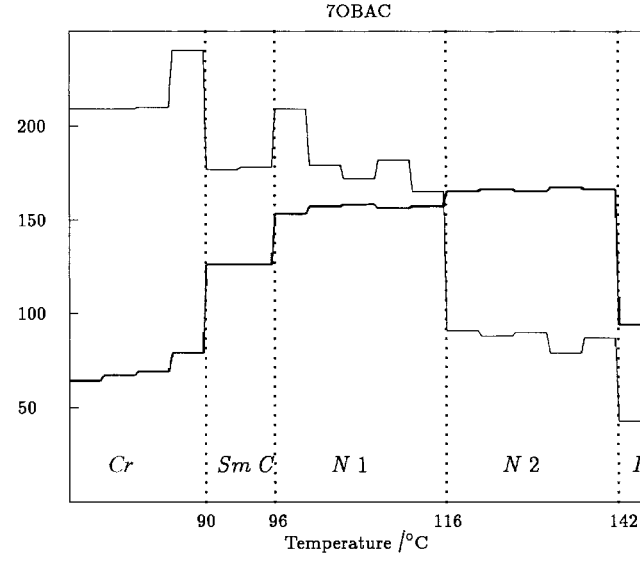

Figure 9. Temperature dependence of the mean intensity (thick line) and of the variance (thin line) of the transmitted light for the images $b(x, y)$ in 7OBAC, on heating. Note the transition between the N_1 and N_2 'subphases', clearly exhibited by the variance. The y-scale is in green tone units.

phase (N_1) to the much more uniform phase (N_2). The curve reporting the mean intensity highlights the phase transitions much more than the textural transition, due to the fact that the intensity of the transmitted light is almost equal for the two 'subphases'. The new method of investigating the optical behaviour of the liquid crystal cell allows a detection of the textural transition between the two 'subphases' with a sensitivity comparable with that for the phase transitions from crystal to smectic, smectic to nematic and the nematic to isotropic phase. Comparing the change in variance at the order transition with the corresponding intensity variation, we can conclude that the moments statistic method can be 10 times more sensitive than standard methods based on intensity detection.

Notice that, for the temperature scan under consideration, an intensity sensor for transmitted light would not be able to identify the 'subphase' transition: the low intensity variation at the order transition would be viewed as a fluctuation inside the phase.

It is useful also to evaluate the skewness S and the kurtosis K:

$$S = \frac{M_3}{\sigma^3} \qquad K = \frac{M_4}{\sigma^4} - 3 \tag{8}$$

where σ is the standard deviation. In our case, the skewness S becomes negative at the transition from the smectic to the nematic phase and remains negative till the clearing point, without any substantial variation at the texture transition. The kurtosis K shows a slow increase in the nematic phase till it reaches its highest value (~ 1). Figure 10 reports the behaviour of S and K in comparison with the standard deviation $\sigma = M_2^{1/2}/M_0$, reduced with respect to the mean intensity.

Analogous results can also be obtained in the presence of defects (see figure 2), allowing the application of the new procedure to the detection of texture transitions also in the case when a network of defects is present in the image frame.

In figure 11 the detail of data for the temperature range near the 'subphase' critical transition ($N_1 \rightarrow N_2$) are shown: the transition exhibits a soft character, in the sense that it takes ~ 2 degrees to complete. This fact may be due to the absence of any particular treatment of the cell glasses: on heating, the transition, which is characterized by the disappearance of the light spots from the sandlike texture, can start at slightly different temperatures in different cell regions, due to the presence of different anchoring conditions [20]. From figure 11, the onset temperature of the transition is easily found: we chose for the onset of the transition that temperature at which the variance changed more than 10% from the value of the variance in the N_1 'subphase'. The same

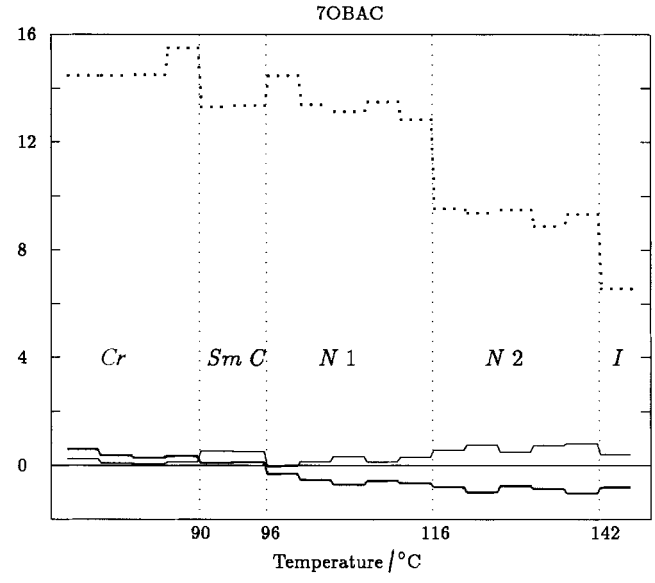

Figure 10. Temperature dependence of the skewness (thick line) and the kurtosis (thin line) for 7OBAC, on heating. The reduced standard deviation σ is also shown (dotted line) for comparison.

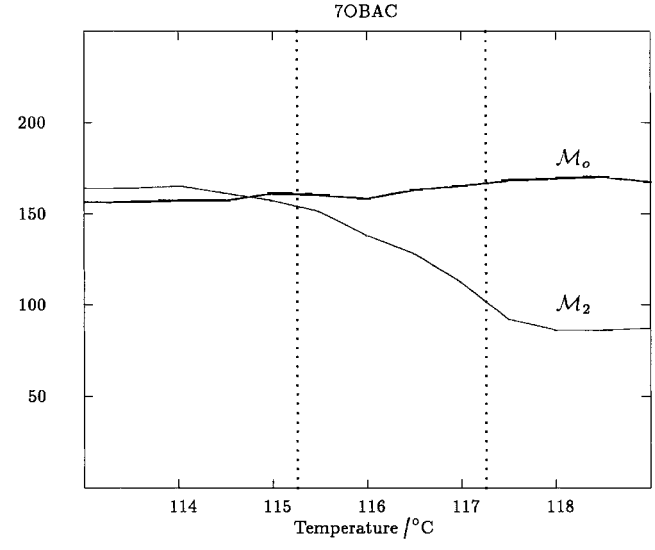

Figure 11. Temperature scanning of 7OBAC on heating near the transition between the N_1 and N_2 'subphases'. The onset and the end of the transition are denoted by the dotted line (see text for explanation). The y-axis scale is in green tone units.

threshold was used to identify the temperature at which the transition would be defined as completed. The total transition range covers about 2 degrees. On cooling, however, the transition N_2 to N_1 is accomplished in less than half a degree.

For 8OBAC, the results of the calculations on a set of histograms obtained by the procedure used for 7OBAC are shown in figure 12. In this case too, the

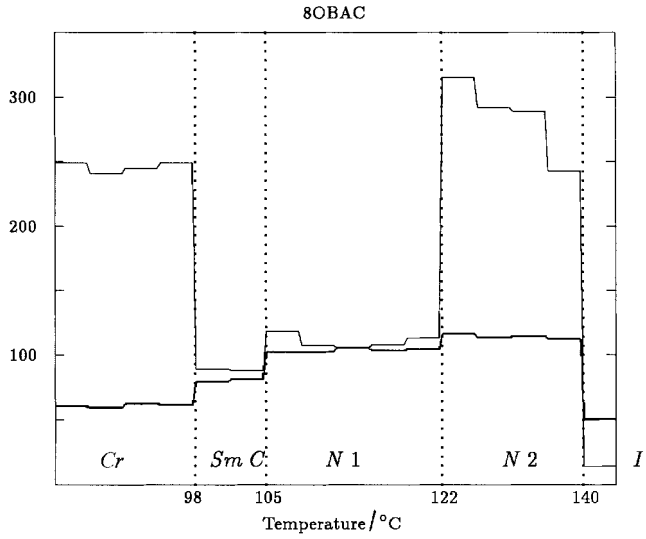

Figure 12. Temperature dependence of the mean intensity (thick line) and of the variance (thin line) of the transmitted light for the images $b(x, y)$ in 8OBAC, on heating. As in 7OBAC, the transition between the N_1 and N_2 'subphases' is clearly exhibited by the variance. The y-scale is in green tone units.

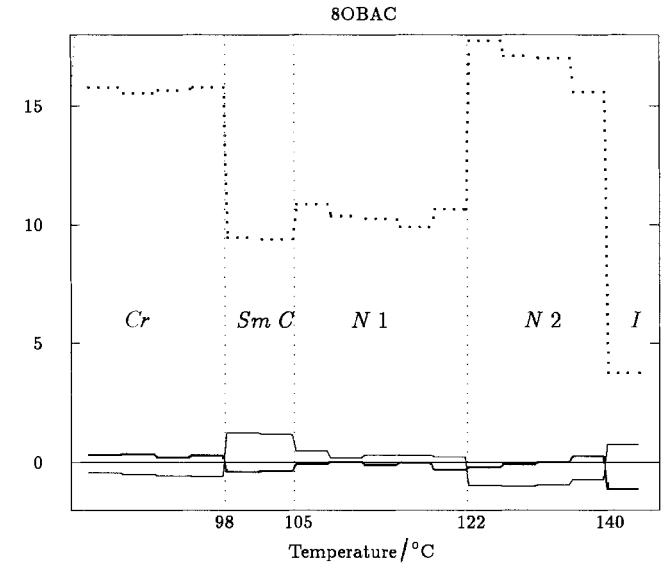

Figure 14. Temperature dependence of the skewness (thick line) and the kurtosis (thin line) for 8OBAC on heating. The reduced standard deviation σ is also shown (dotted line) for comparison. Note the strong variation of the kurtosis in the N_2 phase due to the presence of areas with different birefringence.

mean transmitted light intensity does not change substantially on passing from 'subphase' N_1 to N_2, but we see a strong increase of the variance due to the appearance in N_2 of large areas with different birefringence properties (see figure 13). The presence of different distributions in various regions of the image frame for 'subphase' N_2 is indicated by the high absolute value of the kurtosis, as shown by figure 14 and confirmed by the presence of two peaks in the histogram of the number of pixels N of colour tone b.

Note that for 8OBAC the transition between the two 'subphases' covers a range of ~ 1 degree on heating and $\sim 0{\cdot}2 \rightarrow 0{\cdot}3$ degree on cooling.

As a concluding remark on the detection of the texture transition, let us note that the small difference in the transmitted light intensity on passing from the N_1 'subphase' to the N_2 'subphase' obviously depends on the orientation of the liquid crystal cell with respect to the polarizers. For the measurements on 7OBAC and 8OBAC, we chose the worst orientation for the detection

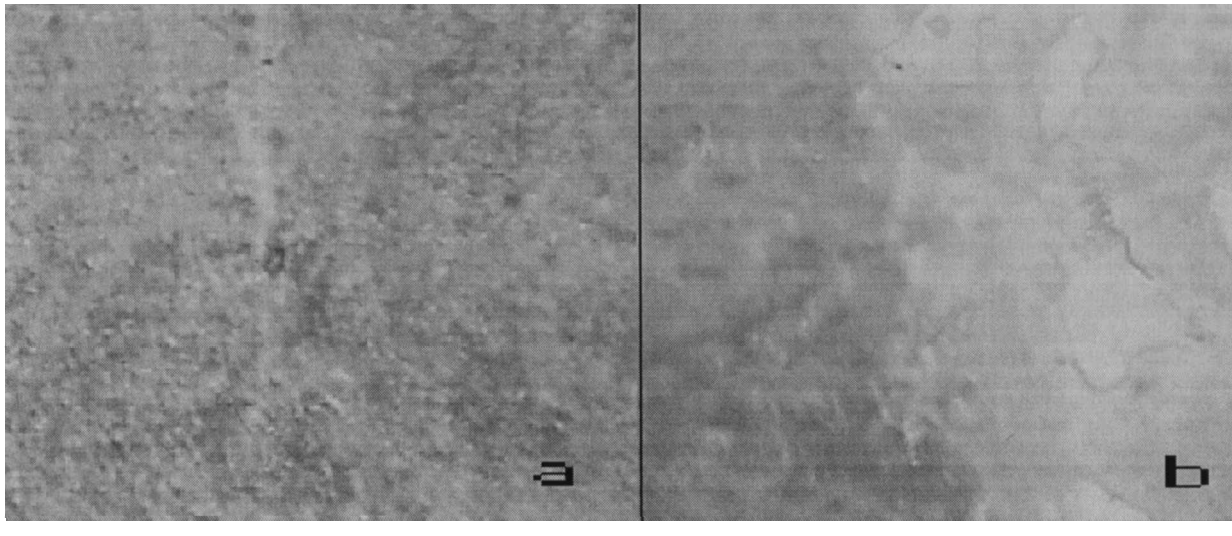

Figure 13. Textures of the N_1 (a) and N_2 (b) 'subphases' of 8OBAC. Note the areas with different birefringence in the phase N_2, producing the increase in the variance in figure 12.

of the transition by simple visual inspection: nevertheless, the statistical results we have presented reveal not only the possibility of detecting the transition, but also the high sensitivity of the method, ensuring its wide applicability.

5. Conclusions

In this paper we have presented a new method of image processing, applied to the analysis of observations made by microscopy (orthoscopic mode) of textural transitions in liquid crystals. We have shown that this approach is reliable and very sensitive for determining the occurrence of smooth transitions, for instance order transitions in one phase, or phase transitions between two phases exhibiting similar structures, such as two smectic phases. In particular, the sensitivity for detecting an order transition in the nematic phase in poorly oriented samples has proved to be enhanced more than 10 times with respect to usual methods.

Thanks are due to P. Montuschi, M. Omini and A. Sanna for useful discussions.

References

[1] Vaughan, R. A., and Osborne, P. (editors), 1991, Pattern Recognition and Image Processing in Physics, 37th Scottish Universities Summer School in Physics, Dundee 1990 (Bristol: Adam Hilger).
[2] Sparavigna, A., Lavrentovich, O. D., and Strigazzi, A., 1994, *Phys. Rev. E*, **49,** 1344.
[3] Kaneko, E., 1986, *Liquid Crystal TV Displays: Principles and Applications of Liquid Crystal Displays* (Tokyo: KTK Scientific Publishers).
[4] Haralick, R. M., 1979, *Proc. IEEE*, **67,** 786.
[5] Weszka, J. S., Dyer, C. R., and Rosenfeld, A., 1976, *IEEE Trans. Syst., Man, Cybern.*, **6,** 369.
[6] Azencott, R., Wang, J., and Younes, L., 1997, *IEEE Trans. Pattern Anal. Mach. Intell.*, **19,** 148.
[7] Haralick, R. M., Shanmugan, K., and Dinstein, I., 1973, *IEEE Trans. Syst., Man, Cybern.*, **3,** 610.
[8] Jähne, B., 1993, *Digital Image Processing* (Berlin: Springer Verlag).
[9] Steurer, J., Giebel, H., and Altner, W., 1986, Proceedings of the 8 DAGM-Symposium, Musterenkennung 1986, edited by G. Hartmann (Berlin: Springer).
[10] Pitas, I., 1993, *Digital Image Processing Algorithms* (Cambridge: Prentice Hall).
[11] Teuber, J., 1993, *Digital Image Processing* (New York: Prentice Hall).
[12] Levine, M. D., 1985, *Vision in Man and Machine* (McGraw-Hill).
[13] Galloway, M. M., 1975, *Comp. Graph. Image process*, **4,** 172.
[14] Gray, G. W., and Jones, B., 1953, *J. chem. Soc.*, **41,** 79.
[15] Herbert, A. J., 1967, *Trans. Faraday. Soc.*, **63,** 555.
[16] De Vries, A., 1970, *Mol. Cryst. liq. Cryst.*, **10,** 31.
[17] Torgova, S. I., Komitov, L., and Strigazzi, A., 1998, *Liq. Cryst.*, **24,** 131.
[18] Frunza, L., Frunza, S., Petrov, M., Sparavigna, A., and Torgova, S. I., 1996, *Mol. Mater.*, **6,** 215.
[19] Petrov, M., Braslau, A., Levelut, A. M., and Durand, G., 1992, *J. Phys. II (Fr.)*, **2,** 1159.
[20] Barbero, G., Komitov, L., Petrov, M., and Strigazzi, A., 1991, *Int. J. mod. Phys. B*, **5,** 2229.
[21] Simova, P., and Petrov, M., 1983, *Phys. Status Solidi A*, **80,** K153.
[22] Petrov, M., and Simova, P., 1985, *J. Phys. D: appl. Phys.*, **18,** 239.
[23] Bryan, R. F., Hartley, P., Miller, R. W., and Ming-Shing, S., 1980, *Mol. Cryst. liq. Cryst.*, **62,** 281.
[24] Neubert, M. E., and De Vries, A., 1987, *Mol. Cryst. liq. Cryst.*, **145,** 1.
[25] Petrov, M., Anachkova, E., Kirov, N., Ratajczak, H., and Baran, J., 1994, *J. mol. Liq.*, **62,** 221.
[26] Coates, D., and Gray, G. W., 1976, *The Microscope*, **24,** 117.